# A Spin-Frustrated Trisradical Trication of PrismCage

Han Han,<sup>1§</sup> Yuheng Huang,<sup>1,2,3</sup>§ Chun Tang,<sup>1</sup> Yiming Liu,<sup>4</sup> Matthew D. Krzyaniak,<sup>1,2,3</sup> Bo Song,<sup>1</sup> Xuesong Li,<sup>1</sup> Guangcheng Wu,<sup>1</sup> Yong Wu,<sup>1</sup> Ruihua Zhang,<sup>1</sup> Yang Jiao,<sup>1</sup> Xingang Zhao,<sup>1</sup> Xiao-Yang Chen,<sup>1</sup> Huang Wu,<sup>1</sup> Charlotte L. Stern,<sup>1</sup> Yuguo Ma,<sup>4</sup> Yunyan Qiu,<sup>5\*</sup> Michael R. Wasielewski,<sup>1,2,3</sup>\* and J. Fraser Stoddart<sup>1,6,7,8</sup>\*

<sup>1</sup>Department of Chemistry, Northwestern University, 2145 Sheridan Road, Evanston, Illinois 60208, United States

<sup>2</sup>Center for Molecular Quantum Transduction, Northwestern University, 2145 Sheridan Road, Evanston, Illinois 60208, United States

<sup>3</sup>Institute for Sustainability and Energy at Northwestern, Northwestern University, Evanston, Illinois 60208, United States

<sup>4</sup>Beijing National Laboratory for Molecular Sciences, Centre for the Soft Matter Science and Engineering,
The Key Lab of Polymer Chemistry & Physics of the Ministry of Education, College of Chemistry and
Molecular Engineering, Peking University, Beijing 100871, China

<sup>5</sup>Department of Chemistry, National University of Singapore, 3 Science Drive 3, Singapore, 117543, Republic of Singapore

<sup>6</sup>Stoddart Institute of Molecular Science, Department of Chemistry, Zhejiang University, Hangzhou 310027, China

<sup>7</sup>ZJU-Hangzhou Global Scientific and Technological Innovation Center, Hangzhou 311215, China <sup>8</sup>School of Chemistry, University of New South Wales, Sydney, NSW 2052, Australia

\*Email: yunyanq@nus.edu.sg; m-wasielewski@northwestern.edu; stoddart@northwestern.edu

ABSTRACT: Organic trisradicals featuring three-fold symmetry have attracted significant interest because of their unique magnetic properties associated with spin frustration. Herein, we describe the synthesis and characterization of a triangular prismshaped organic cage for which we have coined the name PrismCage<sup>6+</sup> and its trisradical trication—TR3(\*+). PrismCage6+ is composed of three 4,4'-bipyridinium dications and two 1,3,5-phenylene units bridged by six methylene groups. In the solid state, **PrismCage**<sup>6+</sup> adopts a highly twisted conformation with close to  $C_3$  symmetry as a result of encapsulating one PF<sub>6</sub><sup>-</sup> anion as a guest. **PrismCage**<sup>6+</sup> undergoes stepwise reduction to its mono-, di- and trisradical cations in MeCN on account of strong electronic communication between its 4,4'-bipyridinium units. TR<sup>3(\*+)</sup>, which is obtained by reduction of **PrismCage**<sup>6+</sup> employing CoCp<sub>2</sub>, adopts a triangular prism-shaped conformation with close to  $C_{2v}$  symmetry in the solid state. Temperature-dependent continuous-wave and nutation frequency-selective EPR spectra of  $TR^{3(+)}$  in frozen N,Ndimethylformamide indicate its doublet ground state. The doublet-quartet energy gap of TR<sup>3(++)</sup> is estimated to be -0.06 kcal mol<sup>-1</sup> and the critical temperature of spin-state conversion is found to be ca. 50 K, suggesting that it displays pronounced spin-frustration at the molecular level. To the best of our knowledge, this example is the first organic radical cage to exhibit spin frustration. The trisradical trication of **PrismCage**<sup>6+</sup> opens up new possibilities for fundamental investigations and potential applications in the fields of both organic cages and spin chemistry.

## Introduction

Stable organic radicals<sup>1</sup> have been emerging as an important class of functional materials that have a variety of applications in fields such as organic electronics, <sup>1d, 2</sup> batteries, <sup>3</sup> and molecular machines<sup>4</sup>. Among them, stable di- and polyradicals are considered to be promising candidates for organic magnets<sup>5</sup> and quantum information materials<sup>6</sup> on account of their intramolecular spin-spin interactions and attractive magnetic properties. One of the most important prerequisites for achieving these applications is precise control over the electronic and magnetic properties of multi-spin systems. Although numerous diradicals have been investigated<sup>7</sup> to elucidate the principles for designing molecules with desired magnetic properties, the challenges grow significantly when it comes to constructing polyradicals<sup>8</sup> with reference to both molecular designs and synthetic methodologies.

Spin frustration,<sup>9</sup> which refers to competing spin states that cannot be satisfied simultaneously in a multi-spin system, is a crucial concept for the advancement of quantum and condensed-matter physics, encompassing spin glass, spin liquid, and superconducting materials. The phenomenon has been observed mainly in the crystalline lattices of inorganic materials. Spin frustration is a rare occurrence in organic radicals<sup>9b, 10</sup> because of the significant challenge of designing them with the necessary crystalline lattices. Organic trisradicals with electronic constitutions featuring three-fold symmetry have attracted significant research interest on account of their distinctive magnetic exchange properties that are linked to spin frustration. During the past 30 years, a few examples of trisradicals—such as tris-nitroxides,<sup>11</sup> propeller-shaped trisradicals,<sup>12</sup> triangular trisradical macrocycles,<sup>13</sup> and a trisradical  $\pi$ -dimer<sup>14</sup>—have been investigated as simplified Ising models (Figure 1a) for gaining insight into spin frustration within organic three-spin systems. All these trisradicals display doublet ground states, while a few of them<sup>11a, 12b, 13a, 13c, 14</sup> have been characterized unambiguously as exhibiting spin frustration at the molecular level. Furthermore, the equilateral triangular constitutions

(Figure 1a) of the trisradicals with spin-frustrated doublet ground states are likely to undergo Jahn–Teller distortion, <sup>12a, 13b, 15</sup> resulting in lower-energy spin states in isosceles triangular constitutions.

There is still plenty of room for the exploration of trisradicals with stronger spinfrustration. The advent of supramolecular cages 16 has sparked our interest in constructing spin-frustrated compounds using organic radical cages<sup>17</sup>. The well-defined 3D topological constitutions of the cages provide an opportunity to arrange radicals in an orderly manner, facilitating desired spin-spin interactions between radical sites at certain distances. Herein, we describe the design, synthesis, and characterization of a triangular prism-shaped hexacationic organic cage, for which we have coined the name PrismCage<sup>6+</sup> and its trisradical trication—TR<sup>3(\*+)</sup>. This PrismCage<sup>6+</sup> is obtained (Figure 1b) by incorporating redox-active building blocks—4,4'-bipyridinium dications (BIPY<sup>2+</sup>)—into a triangular prism-shaped cage with  $D_{3h}$  symmetry. This cage is capped with two 1,3,5-trimethylenebenzene units, which are small enough to facilitate electronic communication between three BIPY<sup>2+</sup> units as well as enhance the magnetic exchange coupling in the case of TR<sup>3(++)</sup>. Temperature-dependent <sup>19</sup>F NMR spectra reveal that PrismCage<sup>6+</sup> is able to encapsulate one PF<sub>6</sub><sup>-</sup> anion in CD<sub>3</sub>CN, exhibiting large association constants of greater than  $4.9\times10^4~\text{M}^{-1}$  at temperatures below 40 °C. In the solid-state superstructures, **PrismCage**<sup>6+</sup> adopts highly twisted conformations with close to  $C_3$  symmetry in response to the guest molecule—the PF<sub>6</sub> anion, hence leading to the presence of a pair of enantiomers of host-guest complexes with (P)- and (M)-helicities. Cyclic voltammetry (CV), differential pulse voltammetry (DPV) and UV-Vis-NIR titration indicate a stepwise reduction of PrismCage<sup>6+</sup> to its mono-, di- and trisradical cations. On reducing the three BIPY<sup>2+</sup> units in **PrismCage<sup>6+</sup>** to BIPY<sup>++</sup>, **TR<sup>3(++)</sup>** is obtained (Figure 1c) and characterized by X-ray crystallography and EPR spectroscopy.  $TR^{3(\bullet+)}$  adopts a triangular prism-shaped constitution with close to  $C_{2v}$  symmetry in the solid state on account of the planarization of the BIPY\*+ units. The N-N distances

between the three BIPY\*+ units are measured to be 5.5, 5.6 and 5.6 Å, respectively, indicating an isosceles constitution caused by the Jahn–Teller effect. Temperature-dependent continuous-wave (CW) and nutation frequency-selective EPR spectra of TR³(\*+) in frozen DMF solutions indicate a doublet ground state for TR³(\*+). The doublet-quartet energy gap of TR³(\*+) is estimated to be -0.06 kcal mol<sup>-1</sup> and the critical temperature of spin-state conversion is found to be as high as ca. 50 K, suggesting that its pronounced spin-frustration character is expressed at the molecular level. All these features render the trisradical trication of **PrismCage**<sup>6+</sup> attractive for fundamental investigations and potential applications in the fields that encompass organic cages and spin chemistry.

## **Results and Discussion**

**Synthesis and Characterization.** The synthetic procedure leading to the preparation of **PrismCage•**6PF<sub>6</sub> is summarized in Scheme 1. The synthesis starts with an S<sub>N</sub>2 substitution between **1•**2PF<sub>6</sub> and (3,5-bis(bromomethyl)phenyl)methanol (**2**), producing **3•**4PF<sub>6</sub> in 67% yield. Bromination of **3•**4PF<sub>6</sub> in HBr/AcOH solution at room temperature affords **4•**4PF<sub>6</sub> in 91% yield. An equimolar mixture of 4,4'-bipyridine and **4•**4PF<sub>6</sub> was dissolved in MeCN and the dilute solution was stirred at 120 °C for 5 days using tetrabutylammonium iodide (TBAI) as catalyst. Purification using reverse-phase column chromatography, followed by a counterion exchange from TFA<sup>-</sup> to PF<sub>6</sub><sup>-</sup>, afforded **PrismCage•**6PF<sub>6</sub> in 17% yield.

The high-resolution ESI-MS of **PrismCage**•6PF<sub>6</sub> reveals (see Supporting Information) a molecular weight of 1572.6911, which is in good agreement with the molecular formula of [**PrismCage**•6PF<sub>6</sub>]. The  $^{1}$ H NMR spectrum of **PrismCage**•6PF<sub>6</sub> recorded in CD<sub>3</sub>CN at 298 K displays (Figure 2a) three peaks ( $\alpha$  /  $\beta$  / 1) in the aromatic region for protons associated with the 4,4'-bipyridinium and 1,3,5-phenylene units and one sharp peak (2) with a chemical shift of 5.70 ppm for protons associated with the methylene groups. The

<sup>13</sup>C NMR spectrum (Figure S6) recorded in CD<sub>3</sub>CN at 298 K shows a total of six carbon resonances. The <sup>1</sup>H and <sup>13</sup>C NMR spectra can be interpreted in terms of **PrismCage**<sup>6+</sup> adopting a conformation with averaged three-fold symmetry in solution. The <sup>19</sup>F NMR spectrum (Figure S12), also recorded in CD<sub>3</sub>CN at 298 K, exhibits two sets of fluorine resonances with <sup>31</sup>P−<sup>19</sup>F coupling constants of 714 and 707 Hz associated with the PF<sub>6</sub><sup>−</sup> anions A and B, respectively. The chemical shifts of the fluorines in the PF<sub>6</sub><sup>−</sup> anion A show significant upfield shifts compared with those of fluorines in the PF<sub>6</sub><sup>−</sup> anion B. The molar ratio of the PF<sub>6</sub><sup>−</sup> anions A and B is calculated to be ca. 1:5. These results indicate the PF<sub>6</sub><sup>−</sup> anions A resides inside the cavity of **PrismCage**<sup>6+</sup>. The complexation of PF<sub>6</sub><sup>−</sup> anions has also been verified (Figure S13) by the <sup>19</sup>F diffusion-ordered spectroscopy (DOSY). The diffusion constants (*D*) extracted from the spectrum reveal that PF<sub>6</sub><sup>−</sup> anion A diffuses at a slower rate (1.05×10<sup>−5</sup> cm<sup>2</sup> s<sup>−1</sup>) than those (2.18×10<sup>−5</sup> cm<sup>2</sup> s<sup>−1</sup>) of the PF<sub>6</sub><sup>−</sup> anions B free in solution, indicating that the PF<sub>6</sub><sup>−</sup> anion A forms a stable host-guest complex with **PrismCage**<sup>6+</sup>.

The complexation between **PrismCage**<sup>6+</sup> and a PF<sub>6</sub><sup>-</sup> anion was confirmed (Figure 3) unambiguously by the solid-state superstructures of **PrismCage**•6PF<sub>6</sub>. Single crystals suitable for X-ray crystallographic analysis were obtained by slow vapor diffusion of  $iPr_2O$  into a MeCN solution of **PrismCage**•6PF<sub>6</sub> after three days. **PrismCage**<sup>6+</sup> encapsulates one PF<sub>6</sub><sup>-</sup> anion and displays (Figure 3a and 3b)  $C_3$  symmetry by adopting a highly twisted conformation in response to the encapsulated guest molecule. The height of this cage is 9.7 Å and the average centroid-to-centroid distances between BIPY<sup>2+</sup> units, which are estimated to be ca. 6.8 Å, are much larger than the average distances (5.8 Å) between the N atoms. The twist angle between the upper and lower phenylene units is as large as 24°, leading to the presence of a pair of enantiomers with (*P*)- and (*M*)-helicities, respectively. These two enantiomers (Figure 3c), which exist as a racemic mixture, are aligned adjacent to each other in a linear manner in the solid-state superstructure.

To establish whether the PF<sub>6</sub><sup>-</sup> anion A is kinetically trapped in **PrismCage**<sup>6+</sup> or is undergoing host-guest equilibration with slow exchange dynamics on the <sup>19</sup>F NMR timescale, temperature-dependent <sup>19</sup>F NMR spectroscopy was carried out (Figure 2b) in the range of -30 to +70 °C. Upon heating, the sharp peaks associated with the PF<sub>6</sub><sup>-</sup> anion A become broadened and the chemical shifts of the PF<sub>6</sub> anions A and B display downfield and upfield shifts, respectively, indicating increasing exchange rates for the PF<sub>6</sub><sup>-</sup> anions inside and outside the cavity of **PrismCage**<sup>6+</sup> at higher temperatures. Simulation (Figure S15) of the line shapes of the spectra recorded at 30, 40, 50, 60 and 70 °C provides rate constants of 9.5, 18.0, 33.0, 58.7 and 109 s<sup>-1</sup>, respectively. The energy barrier  $\Delta G^{\ddagger}$  at 30 °C is estimated to be 16.5 kcal mol<sup>-1</sup> from that rate constant of 9.5 s<sup>-1</sup> using the Eyring equation<sup>18</sup>. The molar ratios estimated from the <sup>19</sup>F NMR spectra of PrismCage•6PF<sub>6</sub> at temperatures between -30 and 30 °C consistently yield an equivalence of 1:5. When heating in the range of 40 to 70 °C, the molar ratios of PF<sub>6</sub><sup>-</sup> anions A and B decrease from 0.98: 5.02 to 0.82: 5.18, suggesting weakened complexation between PrismCage<sup>6+</sup> and PF<sub>6</sub><sup>-</sup> anions at elevated temperatures. The corresponding binding constants also drop down from  $4.9 \times 10^4$  to  $4.0 \times 10^3$  M<sup>-1</sup> within this temperature range. All these results suggest that PF<sub>6</sub><sup>-</sup> anions are undergoing slow exchange on the <sup>19</sup>F NMR timescale between residing inside and remaining outside **PrismCage**<sup>6+</sup> in solution.

**Electrochemistry and UV-Vis-NIR Spectroscopy.** The redox properties of **PrismCage**<sup>6+</sup>, which have been investigated (Figures 4a, 4b, S22 and S23) by CV and DPV, are compared with those of its analogue, i.e., cyclobis(paraquat-*p*-phenylene) tetracation (CBPQT<sup>4+</sup>). The CV traces of CBPQT<sup>4+</sup> comprise two well-defined peaks corresponding to the stepwise reduction of both BIPY<sup>2+</sup> units to BIPY<sup>+</sup> radical cations and then to BIPY(0). In contrast, both CV and DPV data for **PrismCage**<sup>6+</sup> display

(Figures 4b and S23) five reversible reduction peaks with an intensity ratio of approximately 2:1:1:1, indicating (Figure 4a) a stepwise reduction of the BIPY units in PrismCage<sup>6+</sup>. The first two reduction peaks in the case of PrismCage<sup>6+</sup> at -0.18 and -0.25 V versus Ag/AgCl are positively shifted, compared with the first reduction peak (-0.29 V) for CBPQT<sup>4+</sup>, suggesting a pronounced electronic communication between the BIPY units, which leads to the stabilization of the radical cationic species toward oxidation. Moreover, the reduction peaks are more separated between -1.0 and -0.5 V than those in the range, -0.4 to -0.1 V. This result can be attributed to the gradual decrease in the distances between the BIPY units during the reduction process from BIPY<sup>2+</sup> to BIPY<sup>•+</sup>, leading to the planarization of the BIPY units and contraction of the cage. The CV and DPV analyses indicate that the three BIPY units in TR3(++) exhibit stronger electronic communication than those in PrismCage<sup>6+</sup>, an observation which favors enhancement of the intramolecular spin-spin coupling between the BIPY\*+ units. It is worth noting that, even although the first reduction peak in the case of PrismCage<sup>6+</sup> involves a two-electron transfer process, it is likely to be a stepwise reduction<sup>19</sup> from PrismCage<sup>6+</sup> to MR<sup>4+(•+)</sup>, then to DR<sup>2+2(•+)</sup>, in conjunction with the associated conformational changes.

The stepwise reduction of **PrismCage**<sup>6+</sup> to  $TR^{3(++)}$  has also been characterized (Figures 4c and S19) by a titration performed on **PrismCage**<sup>6+</sup> in MeCN employing CoCp<sub>2</sub> ( $E_{red} = -0.91$  V versus Ag/AgCl) and monitored by UV–Vis–NIR spectroscopy. Upon the addition of CoCp<sub>2</sub>, distinctive absorption bands are observed in the wavelength range, 330 to 800 nm. The stoichiometric point, which is associated with  $TR^{3(++)}$ , is confirmed by monitoring the absorption values at 580 nm wherein the absorption reaches its highest value during the titration. The non-linear increase of the absorption values at 580 nm indicates (Figures 4c and S21) that the overall titration can be divided into three stages according to the equivalents of CoCp<sub>2</sub> added to the solution. The stoichiometric point at the end of each stage can be ascribed to the formation of  $MR^{4+(++)}$ ,  $DR^{2+2(++)}$  and  $TR^{3(++)}$ ,

respectively. Furthermore, the intensity ratios of the absorption values either at 380 and 400 nm or at 580 and 605 nm increase during the titration, eventually reaching their highest values upon the formation of pure  $TR^{3(++)}$ , suggesting pronounced electronic communication between the BIPY<sup>++</sup> radical cations. Similar phenomena have been observed (Figures S20 and S21) during the titration of **PrismCage**<sup>6+</sup> employing CoCp<sub>2</sub> in DMF.

In order to elucidate the superstructure of TR<sup>3(++)</sup> in solution, <sup>1</sup>H and <sup>19</sup>F NMR spectra have been recorded for TR<sup>3(•+)</sup>, which is prepared by reducing PrismCage<sup>6+</sup> using 3 equiv of CoCp<sub>2</sub> in degassed CD<sub>3</sub>CN. The <sup>1</sup>H NMR spectrum (Figure S16) of TR<sup>3(++)</sup> recorded at 298 K shows almost no signals except for a sharp peak associated with the protons in CoCp<sub>2</sub><sup>+</sup>. The <sup>19</sup>F NMR spectrum (Figure S17) displays only one set of sharp peaks with a <sup>31</sup>P-<sup>19</sup>F coupling constant of 710 Hz, which can be attributed to the PF<sub>6</sub> anions free in solution. By utilizing one equiv of sodium tetrakis[3,5-bis(trifluoromethyl)phenyl]borate (NaBArF) as the internal standard, the number of the PF<sub>6</sub><sup>-</sup> anions free in solution can be estimated (Figure 4d) to be 6, indicating that the PF<sub>6</sub><sup>-</sup> anion inside the cavity of PrismCage<sup>6+</sup> has been released into solution upon the formation of TR<sup>3(•+)</sup>. X-Ray Crystallography. The solid-state (super)structures of TR•3PF<sub>6</sub> have been characterized by single-crystal X-ray crystallography. Single crystals of TR•3PF<sub>6</sub>, suitable for analysis, were grown under a N<sub>2</sub> atmosphere by evaporating Et<sub>2</sub>O slowly into solutions of MeCN (0.5 mM) overnight. The solid-state (super)structures show (Figure 5a and S29) that the compound crystallizes with three PF<sub>6</sub><sup>-</sup> anions around the cage, an observation which confirms its trisradical tricationic state. A MeCN molecule exists as a guest molecule inside the cavity of TR<sup>3(++)</sup>. The torsional and bending angles for the BIPY\*+ units and the twisting angles between the upper and lower 1,3,5-phenylenes in the solid-state superstructures of TR•3PF<sub>6</sub> are all found to be nearly 0°. The planarization of the BIPY\*+ units endows TR3(\*+) with a larger molecular height of 10.3 Å compared with that (9.7 Å) of PrismCage<sup>6+</sup>. The N-N distances between the three BIPY<sup>\*+</sup> units are

measured (Figure 5d) to be 5.5, 5.6 and 5.6 Å, indicating that  $TR^{3(++)}$  adopts close to  $C_{2v}$  symmetry rather than the expected  $D_{3h}$  symmetry in the solid state. In other words, the triangle drawn by connecting the N atoms as the vertex turns out to be closer to an isosceles rather than equilateral one, with a vertex angle of 59°. This symmetry reduction can be attributed to a Jahn–Teller distortion effect associated with spin frustration. The solid-state superstructures of  $TR^{3(++)}$  reveal (Figure 5e and 5f) a porous network with interconnected 1D channels. Each channel is formed by taking advantage of the strong radical-pairing interactions with a stacking distance of 3.15 Å (Figure 5b) between the BIPY<sup>\*+</sup> units and the  $[\pi\cdots\pi]$  stacking with a packing distance of 3.40 Å (Figure 5c) between the phenylene units in the adjacent cages. The  $C_{2v}$  symmetry of the cages and the slip dislocations between the BIPY<sup>\*+</sup> units in adjacent cages result in distorted hexagonal-shaped channels with diameters in the range of 14 to 19 Å. These unique superstructures provide  $TR^{\bullet}$ 3PF<sub>6</sub> with opportunities for constructing organic radical porous materials.

**EPR Spectroscopy**. X-Band CW-EPR experiments have been carried out to characterize the molecular magnetic properties of  $\mathbf{MR^{4+(++)}}$ ,  $\mathbf{DR^{2+2(++)}}$  and  $\mathbf{TR^{3(++)}}$ . In order to minimize the effect of intramolecular spin-pairing, dilute DMF solutions of these radical cations (1 mM) were prepared for EPR spectroscopy. The EPR spectrum of the frozen DMF solution of  $\mathbf{MR^{4+(++)}}$  exhibits (Figure S24) only a doublet signal. This observation indicates that it is a pure monoradical, rendering it consistent with the results from the UV-Vis-NIR titrations. Temperature-dependent EPR spectra of the frozen DMF solution of  $\mathbf{DR^{2+2(++)}}$  were recorded (Figure S26) in the temperature range of 25 to 150 K. The spectra indicate the presence of a small amount of triplet states of  $\mathbf{DR^{2+2(++)}}$  even at low temperatures. Simulation of the EPR spectrum at 150 K yields an average |D| value of 139 MHz and an average |E| value of 1.9 MHz for  $\mathbf{DR^{2+2(++)}}$ . The |D| value corresponds to an effective spin-spin distance<sup>20</sup> of ca. 6.5 Å for  $\mathbf{DR^{2+2(++)}}$ . This value is a reasonable one, given the fact that the average centroid-to-centroid distances between the BIPY units in  $\mathbf{DR^{2+2(++)}}$  are expected to fall within the range of those in  $\mathbf{PrismCage^{6+}}$  and  $\mathbf{TR^{3(++)}}$ . By

normalizing the EPR spectra at different temperatures, the intensities of triplet signals are observed to increase gradually with increasing temperature, indicating a singlet ground state for  $\mathbf{DR^{2+2(*+)}}$ . The singlet-triplet gap ( $\Delta E_{ST}$ ) is calculated (Figures S30 and Table S2) to be -0.20 kcal mol<sup>-1</sup>, suggesting an antiferromagnetic interaction in  $\mathbf{DR^{2+2(*+)}}$ .

Temperature-dependent EPR spectra of TR<sup>3(•+)</sup> in frozen DMF were recorded (Figure 6a) in the temperature range, 40 to 200 K. The spectrum at 40 K displays only a doublet signal. An observable quantity of the thermally populated quartet state appears at ca. 50 K. This result indicates a doublet ground state and a strong exchange coupling in  $TR^{3(\bullet+)}$ . As a comparison, the critical temperatures of spin-state conversion for triradicals 2,4dimethoxy-1,3,5-benzenetriyltris(*N-tert*-butyl nitroxide) and (+)-NDI- $\Delta^{3(\bullet-)}$ , two<sup>11a,13c</sup> of the few examples that display effective spin-frustration properties, are estimated to be lower than 6.5 and 15 K, respectively. Simulation of the EPR spectrum (Figure 6b) at 200 K yields an average |D| value of 67 MHz and an average |E| value of 0.5 MHz for  $TR^{3(\bullet+)}$ . Moreover, the  $\Delta E_{DO}$  is estimated based on the thermal population of the quartet state. See Supplementary Information for methodology. The relative fractions of S = 3/2 excited state versus S = 1/2 ground state obtained by the simulation (Figure 6c) of CW-EPR spectra at different temperatures provides an estimate ( $-0.06 \text{ kcal mol}^{-1}$ ) for  $\Delta E_{DO}$ . These results indicate much stronger spin-frustration in TR3(++) than that in either the trisnitroxide or (+)-NDI- $\Delta^{3(\bullet-)}$ . We have also attempted to measure the  $\Delta E_{DO}$  employing temperature-dependent EPR spectroscopy for the polycrystalline TR•3PF<sub>6</sub>. The EPR spectra of the solid-state samples,<sup>21</sup> however, display (Figure S24b) exclusively doublet spin-state signals on account of strong intermolecular spin-pairing or antiferromagnetic interactions between TR<sup>3(++)</sup> cages, leading to the absence of quartet spin states originating from intramolecular spin-spin coupling.

Electron spin transient nutation (ESTN) spectroscopy has been employed for assignment of the doublet and quartet spin states observed in the CW-EPR spectra. Nutation frequency-selective EPR measurements were carried out (Figure 7) at 20 and 65 K in conjunction with temperature-dependent CW-EPR measurements to confirm the energy

level orderings of the trisradical tricationic system. Nutation frequencies present in the samples are normalized (Figures 7a and 7b). The feature corresponding to  $\omega_{NUT} = 1.5-1.7$  present in both Figures has been confirmed to be the proton Larmor frequency at ~350 mT prior to normalization. The cross section of the feature related to normalized  $\omega_{NUT} = 1$  ( $m_s = -1/2 \rightarrow m_s = 1/2$  transition) is simulated (Figure 7c) as an S = 1/2 species using a g-tensor wherein g = [2.0035, 2.0034, 2.0024]. The features corresponding to normalized  $\omega_{NUT} = \sqrt{3}$  ( $m_s = -1/2 \rightarrow m_s = 1/2$  transition) and  $\omega_{NUT} = 2$  ( $m_s = -3/2 \rightarrow m_s = -1/2$  or  $m_s = 1/2 \rightarrow m_s = 3/2$  transitions) were simulated assuming the coupled spins behave like an S = 3/2 system. An effective g-tensor, g = [1.9961, 1.9968, 2.0084], and a zero-field splitting |D| = 46 MHz, as well as Euler angles of  $[0^{\circ}, 49^{\circ}, 70^{\circ}]$  relating the zero-field splitting principal axis to that of the g-tensor, were used. The nutation spectra show (Figure 7a) clearly only a  $TR^{3(++)}$  doublet spin state at 20 K and the emergence (Figure 7b) of an additional quartet spin state at 65 K. These results confirm the doublet ground state of  $TR^{3(++)}$  and its intramolecular spin frustration at the molecular level.

**Theoretical Calculations**. In order to gain more insight into the electronic properties of  $TR^{3(+)}$ , calculations have been conducted (Figures 8, S30–34, Tables S2 and S3) for different electronic constitutions of  $TR^{3(+)}$  employing both DFT and CASSCF/NEVPT2 methods. The analysis of the frontier molecular orbitals and spin densities were performed using a multifunctional wave-function analyzer (Multiwfn<sup>22</sup>). The results show (Figure 8) that the electronic constitution with  $D_{3h}$  symmetry has a 0.19 kcal mol<sup>-1</sup> higher energy than that of the isosceles constitution with  $C_{2v}$  symmetry.  $TR^{3(+)}$  with  $C_{2v}$  symmetry, which adopts an isosceles triangular constitution with a vertex angle of 59°, agrees well with the solid-state structure, indicating the Jahn–Teller distortion in  $TR^{3(+)}$ . The occupation numbers of the LUMO in  $TR^{3(+)}$  with  $C_{2v}$  symmetry is 0.92, suggesting a distinctive trisradical character for  $TR^{3(+)}$ . The doublet-quartet energy gaps of  $TR^{3(+)}$  with  $C_{2v}$  and  $D_{3h}$  symmetries are calculated to be -0.18 and -0.09 kcal mol<sup>-1</sup>, respectively, which are also close to that (-0.06 kcal mol<sup>-1</sup>) estimated from temperature-dependent EPR spectra. These results indicate antiferromagnetic spin-spin coupling in  $TR^{3(+)}$ , hence leading to its essential spin frustration.

### **Conclusions**

A triangular prism-shaped hexacationic organic cage, for which we have coined the name **PrismCage**<sup>6+</sup>, and its trisradical trication (TR<sup>3(•+)</sup>), have been designed and synthesized. The PrismCage<sup>6+</sup> is obtained by bridging three BIPY<sup>2+</sup> and two phenylene units using six methylene groups at their 1,3,5-positions. Temperature-dependent <sup>19</sup>F NMR spectra reveal that PrismCage<sup>6+</sup> displays strong association with PF<sub>6</sub><sup>-</sup> anions in solution, with association constants of over  $4.9 \times 10^4$  M<sup>-1</sup> at temperatures below 40 °C. The **PrismCage**<sup>6+</sup> adopts highly twisted conformations with close to  $C_3$  symmetry by encapsulating one PF<sub>6</sub> anion in its solid-state superstructures, resulting in the presence of a pair of enantiomers with (P)- and (M)-helicities. The CV and DPV, combined with UV-Vis-NIR titration, indicate a stepwise reduction of PrismCage<sup>6+</sup> to MR<sup>4+(•+)</sup>, DR<sup>2+2(•+)</sup> and TR<sup>3(•+)</sup>. TR<sup>3(•+)</sup> adopts a triangular prism-shaped conformation with close to  $C_{2v}$  symmetry in solid-state superstructures. The N-N distances between the three BIPY\* units indicate an isosceles constitution for TR<sup>3(++)</sup> caused by the Jahn-Teller effect. Temperature-dependent continuous-wave (CW) and nutation frequency-selective EPR spectra of TR<sup>3(\*+)</sup> in frozen DMF indicate a doublet ground state for TR<sup>3(\*+)</sup>. The doubletquartet energy gap of TR<sup>3(+)</sup> is estimated to be -0.06 kcal mol<sup>-1</sup>, suggesting a strong intramolecular exchange coupling. The trisradical trication of PrismCage<sup>6+</sup> is the first organic cage to exhibit pronounced spin frustration character, making it an attractive platform for investigations in spin chemistry and quantum information science.

#### ASSOCIATED CONTENT

Detailed experimental sections, structural characterization data, EPR characterizations, and theoretical calculations. Crystallographic data for have been deposited in the Cambridge Crystallographic Data Center (CCDC) under accession numbers CCDC:\*\*\*. These data can be obtained free of charge from the CCDC at http://www.ccdc.cam.ac.uk/

data request/cif. The Supporting Information is available free of charge at

https://pubs.acs.org/doi/xxxx/jacsxxx.

**AUTHOR INFORMATION** 

**Corresponding Authors** 

Yunyan Qiu—Department of Chemistry, National University of Singapore, 3 Science

Drive 3, Singapore, 117543, Republic of Singapore.

Email: yunyanq@nus.edu.sg.

Michael R. Wasielewski—Department of Chemistry, Center for Molecular Quantum

Transduction, and Institute for Sustainability and Energy at Northwestern, Northwestern

University, 2145 Sheridan Road, Evanston, Illinois 60208, United States.

Email: m-wasielewski@northwestern.edu.

J. Fraser Stoddart—Department of Chemistry, Northwestern University, 2145 Sheridan

Road, Evanston, Illinois 60208, United States; Stoddart Institute of Molecular Science,

Department of Chemistry, Zhejiang University, Hangzhou 310027, China; ZJU-

Hangzhou Global Scientific and Technological Innovation Center, Hangzhou 311215,

China; School of Chemistry, University of New South Wales, Sydney, NSW 2052,

Australia.

Email: stoddart@northwestern.edu

**Author Contributions** 

§ H.H. and Y.H. contributed equally to this research.

Notes

The authors declare no competing financial interests.

14

#### **ACKNOWLEDGMENTS**

The authors thank Northwestern University for its support of this research. This work was supported by the National Science Foundation under award #CHE-2154627 (M.R.W.). EPR data analysis was supported as part of the Center for Molecular Quantum Transduction (CMQT), an Energy Frontier Research Center funded by the US Department of Energy, Office of Science, Basic Energy Sciences under Award # DE-SC0021314 (M.D.K.). The authors also acknowledge the Quest High-Performance Computing Cluster from Northwestern University and the High-Performance Computing Platform from Peking University for the computational resources.

#### **REFERENCES**

- (1) (a) Ratera, I.; Veciana, J. Playing with Organic Radicals as Building Blocks for Functional Molecular Materials. *Chem. Soc. Rev.* **2012**, *41*, 303–349. (b) Kato, K.; Osuka, A. Platforms for Stable Carbon-Centered Radicals. *Angew. Chem. Int. Ed.* **2019**, *58*, 8978–8986. (c) Tang, B.; Zhao, J.; Xu, J.-F.; Zhang, X. Tuning the Stability of Organic Radicals: From Covalent Approaches to Non-Covalent Approaches. *Chem. Sci.* **2020**, *11*, 1192–1204. (d) Chen, Z. X.; Li, Y.; Huang, F. Persistent and Stable Organic Radicals: Design, Synthesis, and Applications. *Chem* **2021**, *7*, 288–332.
- (2) (a) Ai, X.; Evans, E. W.; Dong, S.; Gillett, A. J.; Guo, H.; Chen, Y.; Hele, T. J. H.; Friend, R. H.; Li, F. Efficient Radical-Based Light-Emitting Diodes with Doublet Emission. *Nature* **2018**, *563*, 536–540. (b) Yuan, D.; Liu, W.; Zhu, X. Design and Applications of Single-Component Radical Conductors. *Chem* **2021**, *7*, 333–357.
- (3) (a) Morita, Y.; Nishida, S.; Murata, T.; Moriguchi, M.; Ueda, A.; Satoh, M.; Arifuku, K.; Sato, K.; Takui, T. Organic Tailored Batteries Materials Using Stable Open-Shell

- Molecules with Degenerate Frontier Orbitals. *Nat. Mater.* **2011**, *10*, 947–951. (b) Chen, Q.; Lv, Y.; Yuan, Z.; Li, X.; Yu, G.; Yang, Z.; Xu, T. Organic Electrolytes for pH-Neutral Aqueous Organic Redox Flow Batteries. *Adv. Funct. Mater.* **2022**, *32*, 2108777.
- (4) (a) Cheng, C.; McGonigal, P. R.; Schneebeli, S. T.; Li, H.; Vermeulen, N. A.; Ke, C.; Stoddart, J. F. An Artificial Molecular Pump. *Nat. Nanotechnol.* **2015**, *10*, 547–553. (b) Qiu, Y.; Song, B.; Pezzato, C.; Shen, D.; Liu, W.; Zhang, L.; Feng, Y.; Guo, Q.-H.; Cai, K.; Li, W.; Chen, H.; Nguyen, M. T.; Shi, Y.; Cheng, C.; Astumian, R. D.; Li, X.; Stoddart, J. F. A Precise Polyrotaxane Synthesizer. *Science* **2020**, *368*, 1247–1253. (c) Cai, K.; Zhang, L.; Astumian, R. D.; Stoddart, J. F. Radical-Pairing-Induced Molecular Assembly and Motion. *Nat. Rev. Chem.* **2021**, *5*, 447–465. (d) Zhang, L.; Qiu, Y.; Liu, W.-G.; Chen, H.; Shen, D.; Song, B.; Cai, K.; Wu, H.; Jiao, Y.; Feng, Y.; Seale, J. S. W.; Pezzato, C.; Tian, J.; Tan, Y.; Chen, X.-Y.; Guo, Q.-H.; Stern, C. L.; Philp, D.; Astumian, R. D.; Goddard, W. A.; Stoddart, J. F. An Electric Molecular Motor. *Nature* **2023**, *613*, 280–286.
- (5) (a) Rajca, A.; Wongsriratanakul, J.; Rajca, S. Magnetic Ordering in an Organic Polymer. *Science* **2001**, *294*, 1503–1505. (b) Mahmood, J.; Park, J.; Shin, D.; Choi, H.-J.; Seo, J.-M.; Yoo, J.-W.; Baek, J.-B. Organic Ferromagnetism: Trapping Spins in the Glassy State of an Organic Network Structure. *Chem* **2018**, *4*, 2357–2369. (c) Phan, H.; Herng, T. S.; Wang, D.; Li, X.; Zeng, W.; Ding, J.; Loh, K. P.; Shen Wee, A. T.; Wu, J. Room-Temperature Magnets Based on 1,3,5-Triazine-Linked Porous Organic Radical Frameworks. *Chem* **2019**, *5*, 1223–1234. (d) Jiang, Q.; Zhang, J.; Mao, Z.; Yao, Y.; Zhao, D.; Jia, Y.; Hu, D.; Ma, Y. Room-Temperature Ferromagnetism in Perylene Diimide Organic Semiconductor. *Adv. Mater.* **2022**, *34*, 2108103.
- (6) Wasielewski, M. R.; Forbes, M. D. E.; Frank, N. L.; Kowalski, K.; Scholes, G. D.; Yuen-Zhou, J.; Baldo, M. A.; Freedman, D. E.; Goldsmith, R. H.; Goodson, T.; Kirk, M. L.; McCusker, J. K.; Ogilvie, J. P.; Shultz, D. A.; Stoll, S.; Whaley, K. B. Exploiting

Chemistry and Molecular Systems for Quantum Information Science. *Nat. Rev. Chem.* **2020**, *4*, 490–504.

- (7) (a) Abe, M. Diradicals. *Chem. Rev.* **2013**, *113*, 7011–7088. (b) Kubo, T. Phenalenyl-Based Open-Shell Polycyclic Aromatic Hydrocarbons. *Chem. Rec.* **2015**, *15*, 218–232. (c) Zeng, Z.; Shi, X.; Chi, C.; López Navarrete, J. T.; Casado, J.; Wu, J. Pro-Aromatic and Anti-Aromatic π-Conjugated Molecules: An Irresistible Wish to Be Diradicals. *Chem. Soc. Rev.* **2015**, *44*, 6578–6596. (d) Tan, G.; Wang, X. Isolable Bis(Triarylamine) Dications: Analogues of Thiele's, Chichibabin's, and Müller's Hydrocarbons. *Acc. Chem. Res.* **2017**, *50*, 1997–2006. (e) Dressler, J. J.; Teraoka, M.; Espejo, G. L.; Kishi, R.; Takamuku, S.; Gómez-García, C. J.; Zakharov, L. N.; Nakano, M.; Casado, J.; Haley, M. M. Thiophene and Its Sulfur Inhibit Indenoindenodibenzothiophene Diradicals from Low-Energy Lying Thermal Triplets. *Nat. Chem.* **2018**, *10*, 1134–1140. (f) Han, H.; Zhang, D.; Zhu, Z.; Wei, R.; Xiao, X.; Wang, X.; Liu, Y.; Ma, Y.; Zhao, D. Aromatic Stacking Mediated Spin–Spin Coupling in Cyclophane-Assembled Diradicals. *J. Am. Chem. Soc.* **2021**, *143*, 17690–17700.
- (8) (a) Rajca, A. From High-Spin Organic Molecules to Organic Polymers with Magnetic Ordering. *Chem. Eur. J.* **2002**, *8*, 4834–4841. (b) Liu, C.; Ni, Y.; Lu, X.; Li, G.; Wu, J. Global Aromaticity in Macrocyclic Polyradicaloids: Hückel's Rule or Baird's Rule? *Acc. Chem. Res.* **2019**, *52*, 2309–2321. (c) Yang, X.; Zhang, D.; Liao, Y.; Zhao, D. Toward an Air-Stable Triradical with Strong Spin Coupling: Synthesis of Substituted Truxene-5,10,15-Triyl. *J. Org. Chem.* **2020**, *85*, 5761–5770.
- (9) (a) Balents, L. Spin Liquids in Frustrated Magnets. *Nature* **2010**, *464*, 199–208. (b) Ganin, A. Y.; Takabayashi, Y.; Jeglič, P.; Arčon, D.; Potočnik, A.; Baker, P. J.; Ohishi, Y.; McDonald, M. T.; Tzirakis, M. D.; McLennan, A.; Darling, G. R.; Takata, M.; Rosseinsky, M. J.; Prassides, K. Polymorphism Control of Superconductivity and

Magnetism in Cs<sub>3</sub>C<sub>60</sub> Close to the Mott Transition. *Nature* **2010**, *466*, 221–225. (c) Broholm, C.; Cava, R. J.; Kivelson, S. A.; Nocera, D. G.; Norman, M. R.; Senthil, T. Quantum Spin Liquids. *Science* **2020**, *367*, eaay0668. (d) Chamorro, J. R.; McQueen, T. M.; Tran, T. T. Chemistry of Quantum Spin Liquids. *Chem. Rev.* **2021**, *121*, 2898–2934.

(10)(a) Pratt, F. L.; Baker, P. J.; Blundell, S. J.; Lancaster, T.; Ohira-Kawamura, S.; Baines, C.; Shimizu, Y.; Kanoda, K.; Watanabe, I.; Saito, G. Magnetic and Non-Magnetic Phases of a Quantum Spin Liquid. *Nature* **2011**, *471*, 612–616. (b) Postulka, L.; Winter, S. M.; Mihailov, A. G.; Mailman, A.; Assoud, A.; Robertson, C. M.; Wolf, B.; Lang, M.; Oakley, R. T. Spin Frustration in an Organic Radical Ion Salt Based on a Kagome-Coupled Chain Structure. *J. Am. Chem. Soc.* **2016**, *138*, 10738–10741. (c) Takabayashi, Y.; Menelaou, M.; Tamura, H.; Takemori, N.; Koretsune, T.; Štefančič, A.; Klupp, G.; Buurma, A. J. C.; Nomura, Y.; Arita, R.; Arčon, D.; Rosseinsky, M. J.; Prassides, K. π-Electron S = ½ Quantum Spin-Liquid State in an Ionic Polyaromatic Hydrocarbon. *Nat. Chem.* **2017**, *9*, 635–643.

(11)(a) Fujita, J.; Tanaka, M.; Suemune, H.; Koga, N.; Matsuda, K.; Iwamura, H. Antiferromagnetic Exchange Interaction Among the Three Spins Placed in an Isosceles Triangular Configuration in 2,4-Dimethoxy-1,3,5-Benzenetriyltris(*N*-Tert-Butyl Nitroxide). *J. Am. Chem. Soc.* **1996**, *118*, 9347–9351. (b) Itoh, T.; Matsuda, K.; Iwamura, H.; Hori, K. Tris[*p*-(*N*-Oxyl-*N*-Tert-Butylamino)Phenyl]Amine, -Methyl, and -Borane Have Doublet, Triplet, and Doublet Ground States, Respectively. *J. Am. Chem. Soc.* **2000**, *122*, 2567–2576. (c) Suzuki, S.; Nagata, A.; Kuratsu, M.; Kozaki, M.; Tanaka, R.; Shiomi, D.; Sugisaki, K.; Toyota, K.; Sato, K.; Takui, T.; Okada, K. Trinitroxide-Trioxytriphenylamine: Spin-State Conversion from Triradical Doublet to Diradical Cation Triplet by Oxidative Modulation of a π-Conjugated System. *Angew. Chem. Int. Ed.* **2012**, *51*, 3193–3197.

- (12)(a) Kodama, T.; Aoba, M.; Hirao, Y.; Rivero, S. M.; Casado, J.; Kubo, T. Molecular and Spin Structures of a through-Space Conjugated Triradical System. *Angew. Chem. Int. Ed.* **2022**, *61*, e202200688. (b) Tang, S.; Ruan, H.; Hu, Z.; Zhao, Y.; Song, Y.; Wang, X. A Cationic Sulfur-Hydrocarbon Triradical with an Excited Quartet State. *Chem. Commun.* **2022**, *58*, 1986–1989.
- (13)(a) Kurata, R.; Sakamaki, D.; Uebe, M.; Kinoshita, M.; Iwanaga, T.; Matsumoto, T.; Ito, A. Isolable Triradical Trication of Hexaaza[16]Paracyclophane with Embedded 9,10-Anthrylenes: A Frustrated Three-Spin System. *Org. Lett.* **2017**, *19*, 4371–4374. (b) Lu, X.; Lee, S.; Hong, Y.; Phan, H.; Gopalakrishna, T. Y.; Herng, T. S.; Tanaka, T.; Sandoval-Salinas, M. E.; Zeng, W.; Ding, J.; Casanova, D.; Osuka, A.; Kim, D.; Wu, J. Fluorenyl Based Macrocyclic Polyradicaloids. *J. Am. Chem. Soc.* **2017**, *139*, 13173–13183. (c) Wu, Y.; Krzyaniak, M. D.; Stoddart, J. F.; Wasielewski, M. R. Spin Frustration in the Triradical Trianion of a Naphthalenediimide Molecular Triangle. *J. Am. Chem. Soc.* **2017**, *139*, 2948–2951.
- (14) Wang, W.; Ma, X.-H.; Liu, M.; Tang, S.; Ding, X.; Zhao, Y.; Tan, Y.-Z.; Kertesz, M.; Wang, X. A Triply Negatively Charged Nanographene Bilayer with Spin Frustration. *Angew. Chem. Int. Ed.* **2022**, *62*, e202217788.
- (15) Kahn, O. Competing Spin Interactions and Degenerate Frustration for Discrete Molecular Species. *Chem. Phys. Lett.* **1997**, *265*, 109–114.
- (16)(a) Zhang, G.; Mastalerz, M. Organic Cage Compounds—from Shape-Persistency to Function. *Chem. Soc. Rev.* **2014**, *43*, 1934–1947. (b) Hasell, T.; Cooper, A. I. Porous Organic Cages: Soluble, Modular and Molecular Pores. *Nat. Rev. Mater.* **2016**, *1*, 16053. (c) Samanta, D.; Galaktionova, D.; Gemen, J.; Shimon, L. J. W.; Diskin-Posner, Y.; Avram, L.; Král, P.; Klajn, R. Reversible Chromism of Spiropyran in the Cavity of a

Flexible Coordination Cage. *Nat. Commun.* **2018**, *9*, 641. (d) Rizzuto, F. J.; von Krbek, L. K. S.; Nitschke, J. R. Strategies for Binding Multiple Guests in Metal–Organic Cages. *Nat. Rev. Chem.* **2019**, *3*, 204–222. (e) Jiao, T.; Wu, G.; Zhang, Y.; Shen, L.; Lei, Y.; Wang, C.-Y.; Fahrenbach, A. C.; Li, H. Self-Assembly in Water with *N*-Substituted Imines. *Angew. Chem. Int. Ed.* **2020**, *59*, 18350–18367. (f) Takezawa, H.; Shitozawa, K.; Fujita, M. Enhanced Reactivity of Twisted Amides inside a Molecular Cage. *Nat. Chem.* **2020**, *12*, 574–578. (g) Zhao, X.; Liu, Y.; Zhang, Z.-Y.; Wang, Y.; Jia, X.; Li, C. One-Pot and Shape-Controlled Synthesis of Organic Cages. *Angew. Chem. Int. Ed.* **2021**, *60*, 17904–17909. (h) Pavlović, R. Z.; Zhiquan, L.; Finnegan, T. J.; Waudby, C. A.; Wang, X.; Gunawardana, V. W. L.; Zhu, X.; Wong, C. M.; Hamby, T.; Moore, C. E.; Hoefer, N.; McComb, D. W.; Sevov, C. S.; Badjić, J. D. Closed Aromatic Tubes—Capsularenes. *Angew. Chem. Int. Ed.* **2022**, *61*, e202211304.

(17)(a) Nakabayashi, K.; Ozaki, Y.; Kawano, M.; Fujita, M. A Self-Assembled Spin Cage. *Angew. Chem. Int. Ed.* **2008**, *47*, 2046–2048. (b) Huang, B.; Mao, L.; Shi, X.; Yang, H.-B. Recent Advances and Perspectives on Supramolecular Radical Cages. *Chem. Sci.* **2021**, *12*, 13648–13663. (c) Jiao, T.; Qu, H.; Tong, L.; Cao, X.; Li, H. A Self-Assembled Homochiral Radical Cage with Paramagnetic Behaviors. *Angew. Chem. Int. Ed.* **2021**, *60*, 9852–9858. (d) Wu, S.; Ni, Y.; Han, Y.; Hou, X.; Wang, C.; Hu, W.; Wu, J. Hückel- and Baird-Type Global Aromaticity in a 3D Fully Conjugated Molecular Cage. *Angew. Chem. Int. Ed.* **2022**, *61*, e202115571.

(18) The Eyring equation is written in a linearized form:  $ln\frac{k}{T} = -\frac{\Delta H^{\ddagger}}{R}\frac{1}{T} + \frac{\Delta S^{\ddagger}}{R} + ln\frac{k_B}{h}$ . Thus ln(k/T) is plotted versus 1/T. The enthalpy of activation  $(\Delta H^{\ddagger})$  and the entropy of activation  $(\Delta S^{\ddagger})$  are estimated to be 12 kcal mol<sup>-1</sup> and -0.015 kcal mol<sup>-1</sup> K<sup>-1</sup> from the slope and the intercept, respectively.

- (19)(a) Bellec, N.; Boubekeur, K.; Carlier, R.; Hapiot, P.; Lorcy, D.; Tallec, A. Controlling the Conformation Changes Associated to Electron Transfer Steps through Chemical Substitution: Intriguing Redox Behavior of Substituted Vinylogous TTF. *J. Phys. Chem. A* **2000**, *104*, 9750–9759. (b) Evans, D. H. One-Electron and Two-Electron Transfers in Electrochemistry and Homogeneous Solution Reactions. *Chem. Rev.* **2008**, *108*, 2113–2144. (c) Fortage, J.; Peltier, C.; Nastasi, F.; Puntoriero, F.; Tuyèras, F.; Griveau, S.; Bedioui, F.; Adamo, C.; Ciofini, I.; Campagna, S.; Lainé, P. P. Designing Multifunctional Expanded Pyridiniums: Properties of Branched and Fused Head-to-Tail Bipyridiniums. *J. Am. Chem. Soc.* **2010**, *132*, 16700–16713.
- (20) Minato, M.; Lahti, P. M. Zero-Field Splitting Versus Interelectronic Distance in Triplet Electron Spin Resonance Spectra of Localized Dinitrenes. *J. Phys. Org. Chem.* **1993**, *6*, 483–487.
- (21) Because of the strong radical-pairing interations in the polycrystalline samples of TR•3PF6, we have also explored two strategies to weaken the aggregation of TR<sup>3(\*+)</sup> during the cooling process. (i) The first strategy was to prepare TR•3BArF by counterion exchange of PF6<sup>-</sup> anions using NaBArF. The much larger size of BArF<sup>-</sup> was expected to prevent TR<sup>3(\*+)</sup> from aggregation but failed in the event. (ii) The second strategy was to disperse TR•3PF6 into a liquid crystal or polymer matrix. A liquid crystal, 4-cyano-4'-pentylbiphenyl (5CB), has been used as the matrix to disperse the TR•3PF6. Although TR•3PF6 can be evenly dispersed in 5CB, it still failed to prevent it from aggregating upon cooling.
- (22) Lu, T.; Chen, F. Multiwfn: A Multifunctional Wavefunction Analyzer. *J. Comput. Chem.* **2012**, *33*, 580–592.

# **Captions to Schemes and Figures**

**Scheme 1.** Synthesis of **PrismCage•**6PF<sub>6</sub>. The synthesis starts with an S<sub>N</sub>2 substitution between **1•**2PF<sub>6</sub> and **2**, producing **3•**4PF<sub>6</sub> in 67% yield. Bromination of **3•**4PF<sub>6</sub> in HBr/AcOH solution at room temperature affords **4•**4PF<sub>6</sub> in 91% yield. Cyclization between 4,4'-bipyridine and **4•**4PF<sub>6</sub> in MeCN at 120 °C affords **PrismCage•**6PF<sub>6</sub> in 17% yield.

Figure 1. Molecular design of PrismCage<sup>6+</sup> and its trisradical trication  $TR^{3(\bullet+)}$ . (a) Graphical representation of a simplified Ising model of spin-frustration. The three-spin system with  $D_{3h}$  symmetry which adopts an equilateral triangular electronic constitution can undergo a Jahn–Teller distortion to form an isosceles triangular constitution with  $C_{2v}$  symmetry. (b) PrismCage<sup>6+</sup>, a hexacationic organic cage with  $D_{3h}$  symmetry, is designed by bridging two phenylene and three BIPY<sup>2+</sup> building blocks employing six methylene groups as the linkers. (c) Graphical representation of the structures of PrismCage<sup>6+</sup> and its trisradical trication  $TR^{3(\bullet+)}$ .

**Figure 2.** The  $^{1}$ H and  $^{19}$ F NMR spectra of **PrismCage**•6PF<sub>6</sub>. (a) The  $^{1}$ H NMR spectrum (500 MHz, CD<sub>3</sub>CN, 298 K) of **PrismCage**•6PF<sub>6</sub> (0.2 mM) displays three peaks (α / β / 1) in the aromatic region and one sharp peak (2) with a chemical shift of 5.70 ppm. It suggests that **PrismCage**<sup>6+</sup> adopts a conformation with averaged three-fold symmetry in solution. (b) Temperature-dependent  $^{19}$ F NMR spectra (600 MHz, CD<sub>3</sub>CN) of **PrismCage**•6PF<sub>6</sub> (0.2 mM). The molar ratios estimated from the  $^{19}$ F NMR spectra at temperatures between  $^{-30}$  and  $^{30}$  C consistently yield a value of 1:5. When heating from 40 to 70 °C, the molar ratios of PF<sub>6</sub><sup>-</sup>A and B decrease from 0.98 : 5.02 to 0.82 : 5.18, and the corresponding binding constants decrease from  $^{4.9}$ ×10<sup>4</sup> to  $^{4.0}$ ×10<sup>3</sup> M<sup>-1</sup>,

suggesting weakened complexation between **PrismCage**<sup>6+</sup> and PF<sub>6</sub><sup>-</sup> anions at elevated temperatures. Simulation (Figure S15) of the line shapes of the spectra recorded at 30, 40, 50, 60 and 70 °C provides rate constants of 9.5, 18.0, 33.0, 58.7 and 109 s<sup>-1</sup>, respectively. The energy barrier  $\Delta G^{\ddagger}$  at 30 °C is estimated to be 16.5 kcal mol<sup>-1</sup> from the rate constant of 9.5 s<sup>-1</sup> using the Eyring equation.

Figure 3. Tubular representations of the solid-state superstructures of PrismCage•6PF<sub>6</sub>.

(a) Side-on and (b) top-down views of the solid-state superstructures of PrismCage•6PF<sub>6</sub>.

PrismCage<sup>6+</sup> encapsulates one PF<sub>6</sub><sup>-</sup> anion and displays close to C<sub>3</sub> symmetry by adopting a highly twisted triangular prism-shaped conformation in response to the guest molecule. The twisting angle between the upper and lower phenylene rings is as large as 24°, leading to the presence of a pair of enantiomers with (P)- and (M)-helicities, respectively.

(c) Packing modes of the solid-state superstructures of PrismCage•6PF<sub>6</sub>. Two enantiomers exist as a racemic mixture and are aligned adjacent to each other in the solid-state superstructures.

**Figure 4.** Electrochemistry and UV-Vis-NIR spectroscopy. (a) Structural formulas of **PrismCage**<sup>6+</sup> and the formation of its radical cations during the redox process. (b) The CV and DPV of **PrismCage**<sup>6+</sup> and CBPQT<sup>4+</sup>. (c) UV-Vis-NIR Titration on **PrismCage**<sup>6+</sup> in MeCN employing CoCp<sub>2</sub> as the reducing reagent. The titration displays three stages corresponding to the formation of **MR**<sup>4+(\*+)</sup>, **DR**<sup>2+2(\*+)</sup> and **TR**<sup>3(\*+)</sup>, respectively. (d) The <sup>19</sup>F NMR spectrum (564 MHz, CD<sub>3</sub>CN, 298 K) of **TR**<sup>3(\*+)</sup> (0.2 mM), which was prepared by reducing **PrismCage**<sup>6+</sup> using 3 equiv of CoCp<sub>2</sub> in degassed CD<sub>3</sub>CN. An equimolar amount of NaBArF was utilized as the internal standard to estimate the number of the PF<sub>6</sub><sup>-</sup> anions free in solution.

**Figure 5.** Tubular representations of the solid-state superstructures of  $TR ext{-}3PF_6$ . (a) Sideon and (d) top-down views of the solid-state superstructures of  $TR ext{-}3PF_6$ . The compound crystallizes with three  $PF_6^-$  anions around the cage.  $TR^{3( ext{-}+)}$  encapsulates one MeCN as the guest molecule and displays  $C_{2v}$  symmetry. (c) Two BIPY $^{ ext{-}+}$  units from adjacent cages display radical-pairing interactions with a stacking distance of 3.15 Å. (d) Two phenylene units from adjacent cages display  $[\pi \cdots \pi]$  stacking with a packing distance of 3.40 Å. (e) The solid-state superstructure of  $TR^{3( ext{-}+)}$  reveals a porous network with interconnected 1D channels. (f) Graphical representation of hexagonal 1D channels.

Figure 6. (a) Temperature-dependent X-band CW-EPR spectra of  $TR^{3(\bullet+)}$  recorded in DMF (1 mM) in the range of 40 to 200 K. (b) Simulation of the EPR spectra of  $TR^{3(\bullet+)}$  at 200 K. g-Tensor = [1.9961, 1.9988, 2.0080]. |D| = 67 MHz. |E| = 0.5 MHz. DFrame = [0°, 49°, 70°]. (c) The relative fraction (blue dots) of S = 3/2 excited states versus S = 1/2 ground states obtained by simulation of CW-EPR spectra at different temperatures. Fitting the plot (red line) employing Boltzmann statistics provides an estimate (-0.06 kcal mol<sup>-1</sup>) for  $\Delta E_{DQ}$ .

Figure 7. Nutation frequency-selective EPR spectra of  $TR^{3(-+)}$  recorded in DMF (1 mM) at (a) 20 K and (b) 65 K. (c) Plots of the cross sections (black dots) at normalized nutation frequency ( $\omega_{NUT} = 1, \sqrt{3}, 2$ ) and their corresponding simulation curves (red lines).

**Figure 8.** Calculated spin densities and doublet-quartet energy gaps ( $\Delta E_{DQ}$ ) for two different electronic constitutions of  $\mathbf{TR^{3(+)}}$  at the UM06-2X/6-31G(d,p) level. The doublet-quartet energy gaps of  $\mathbf{TR^{3(+)}}$  with  $C_{2v}$  and  $D_{3h}$  symmetries are calculated to be -0.18 and -0.09 kcal mol<sup>-1</sup>, respectively. The energy level of  $\mathbf{TR^{3(+)}}$  with  $C_{2v}$  symmetry is 0.19 kcal mol<sup>-1</sup> lower than that of  $\mathbf{TR^{3(+)}}$  with  $D_{3h}$  symmetries.

Scheme 1

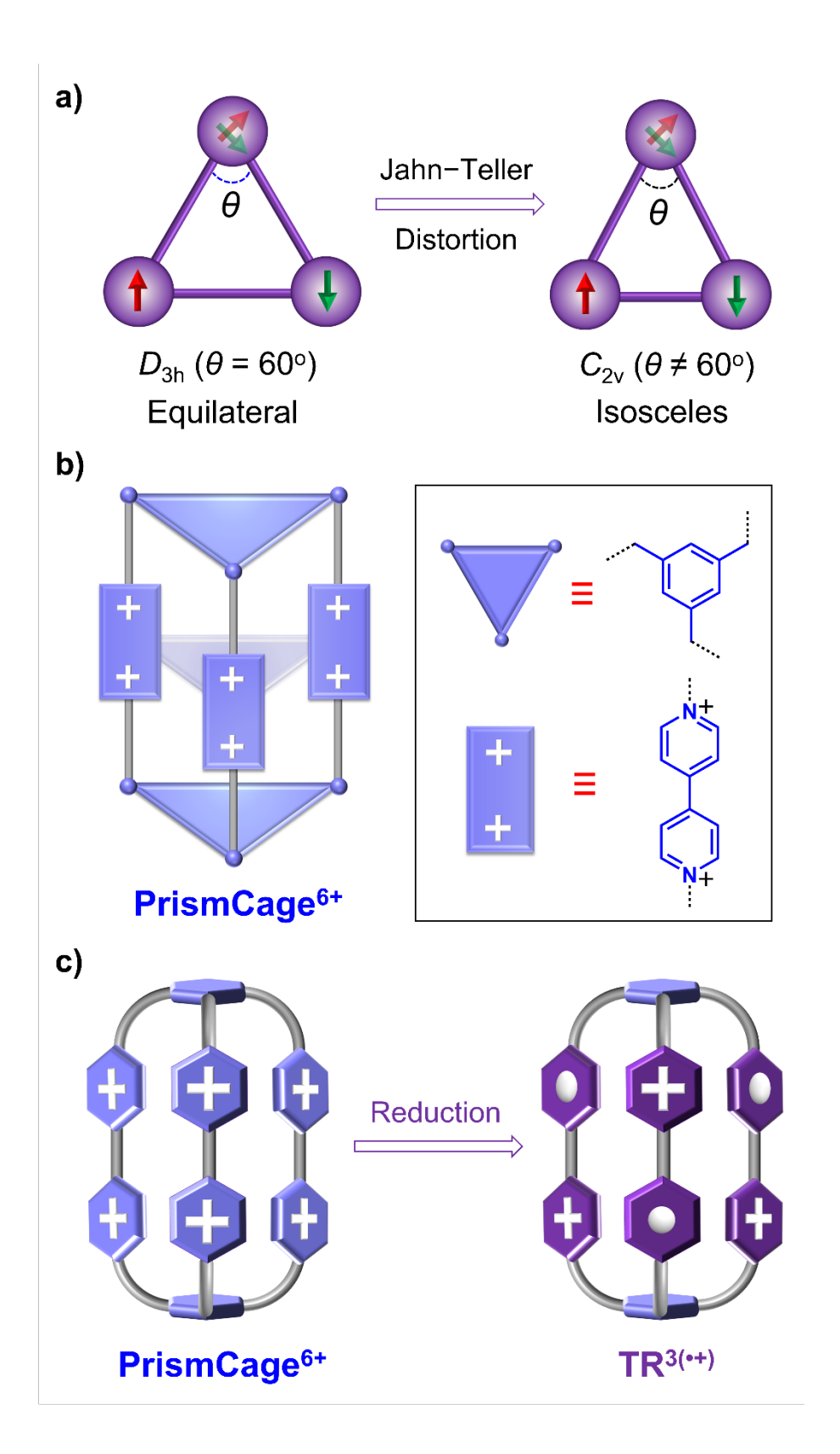


Figure 1

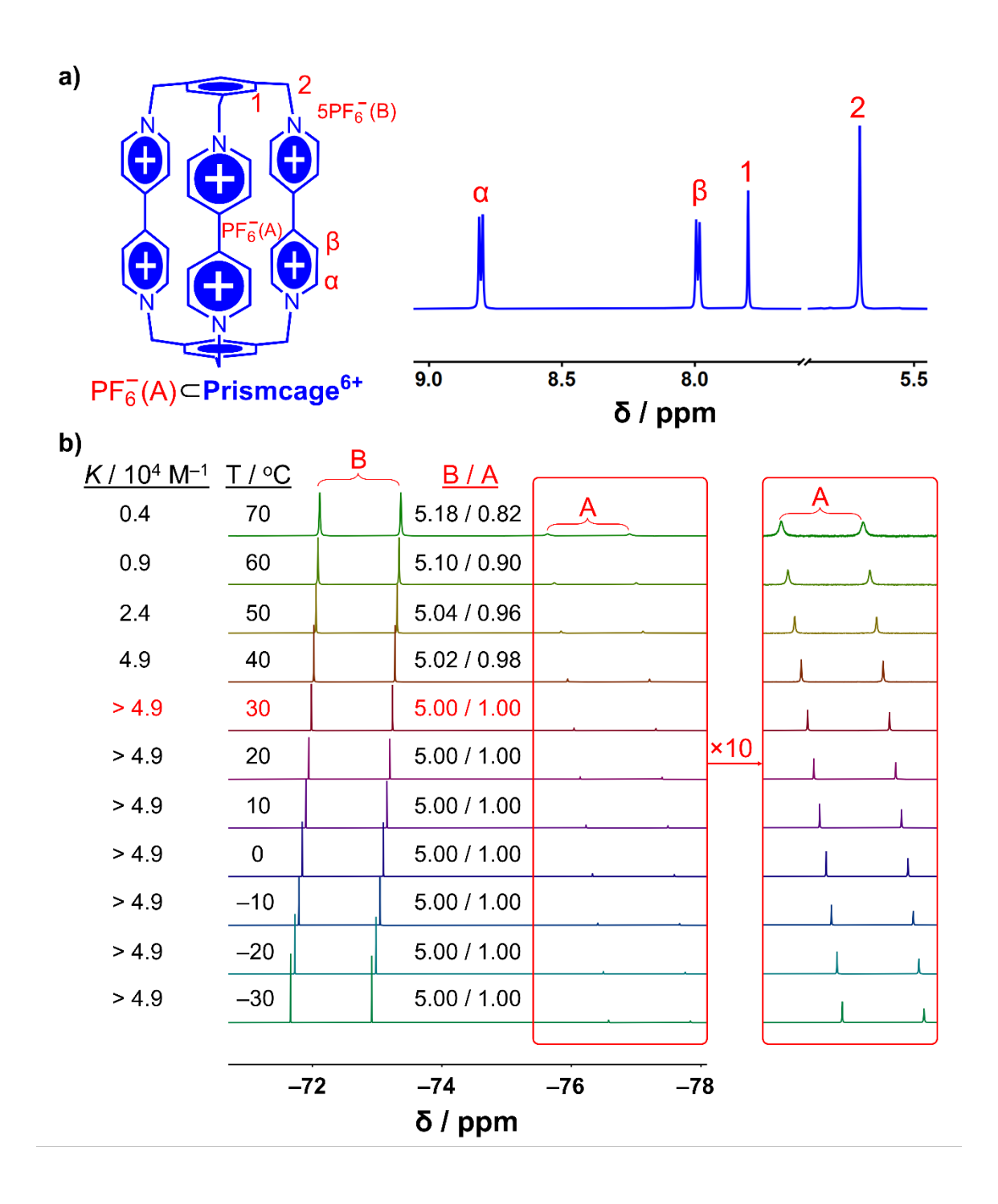


Figure 2

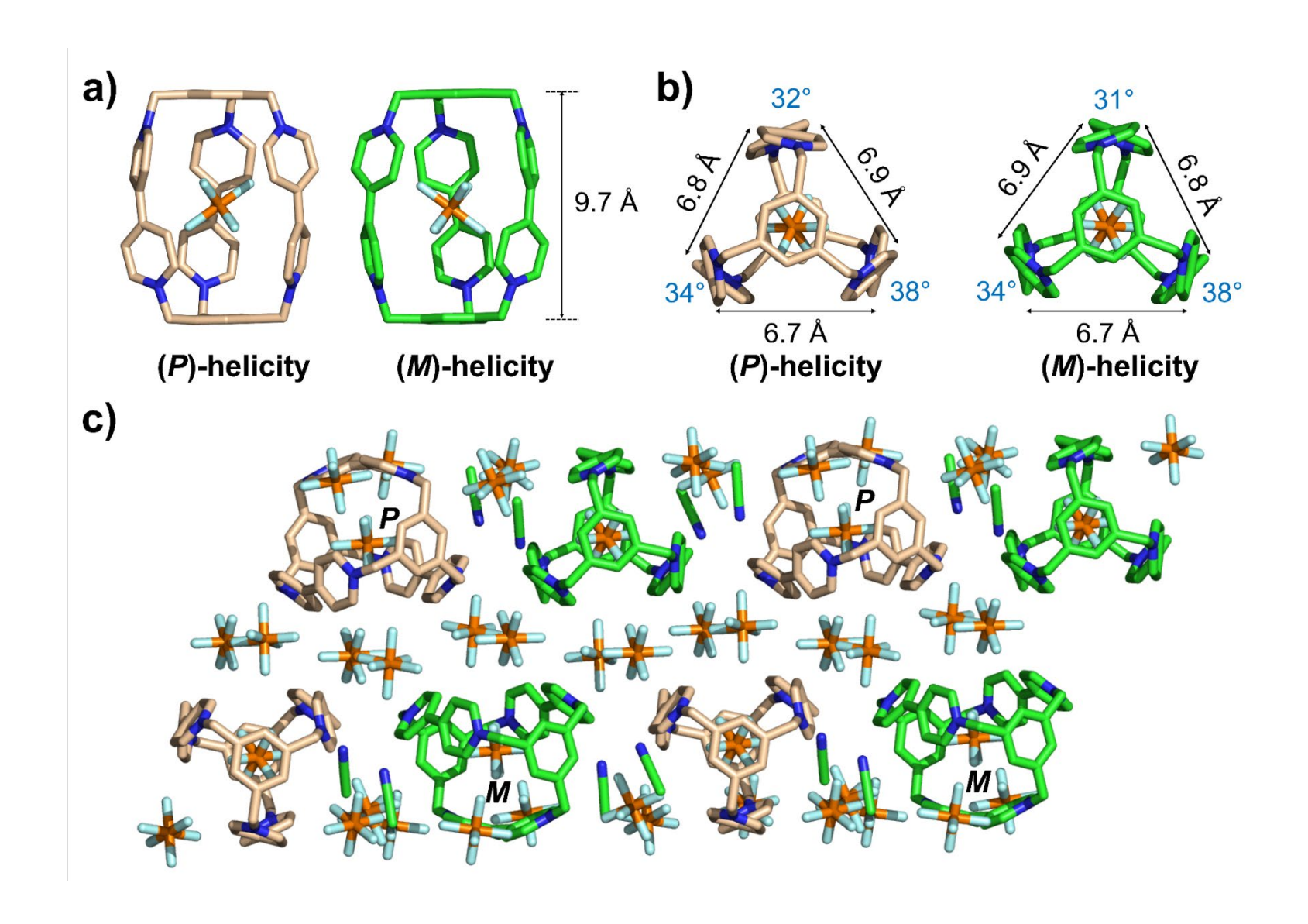


Figure 3

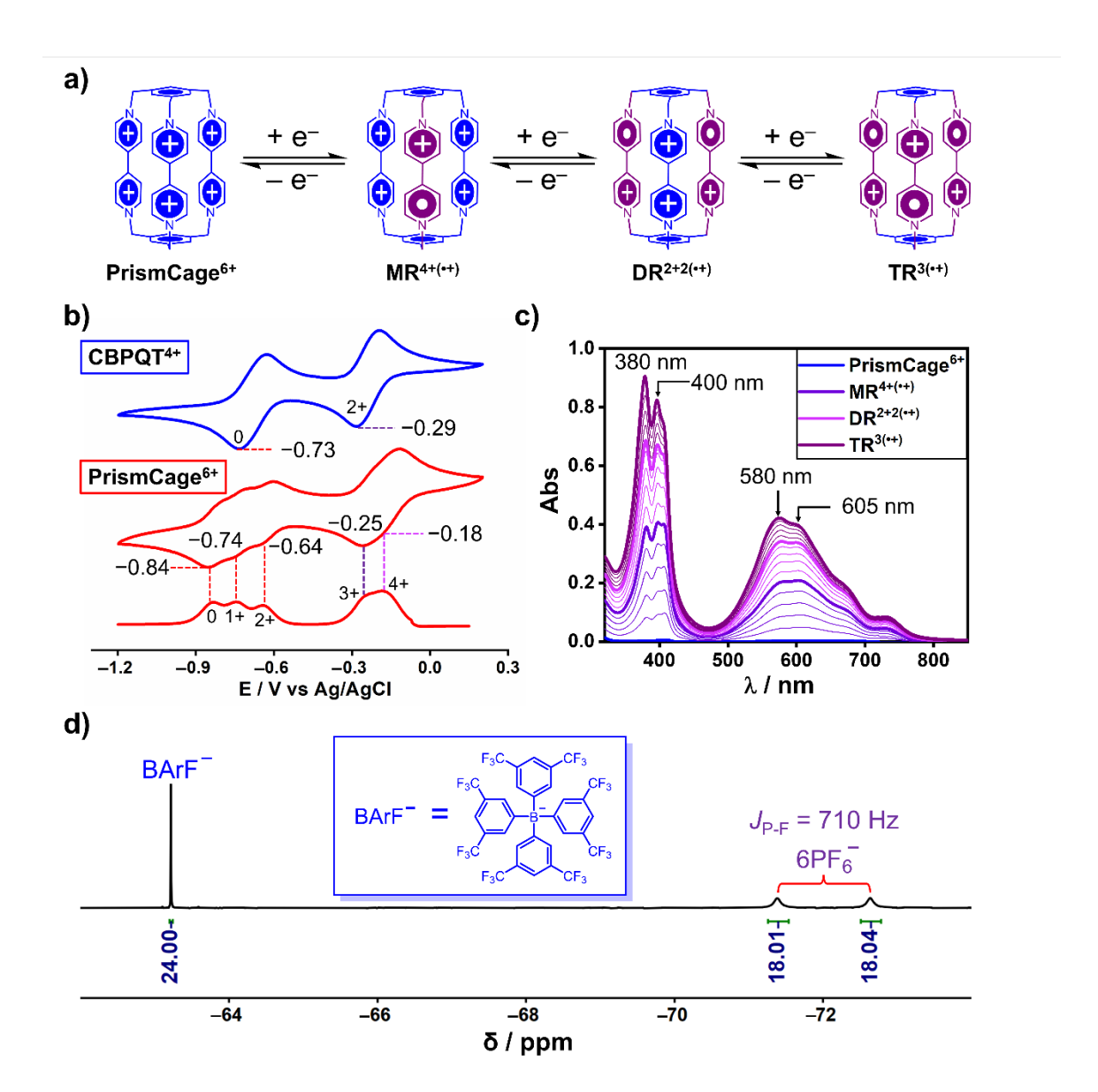


Figure 4

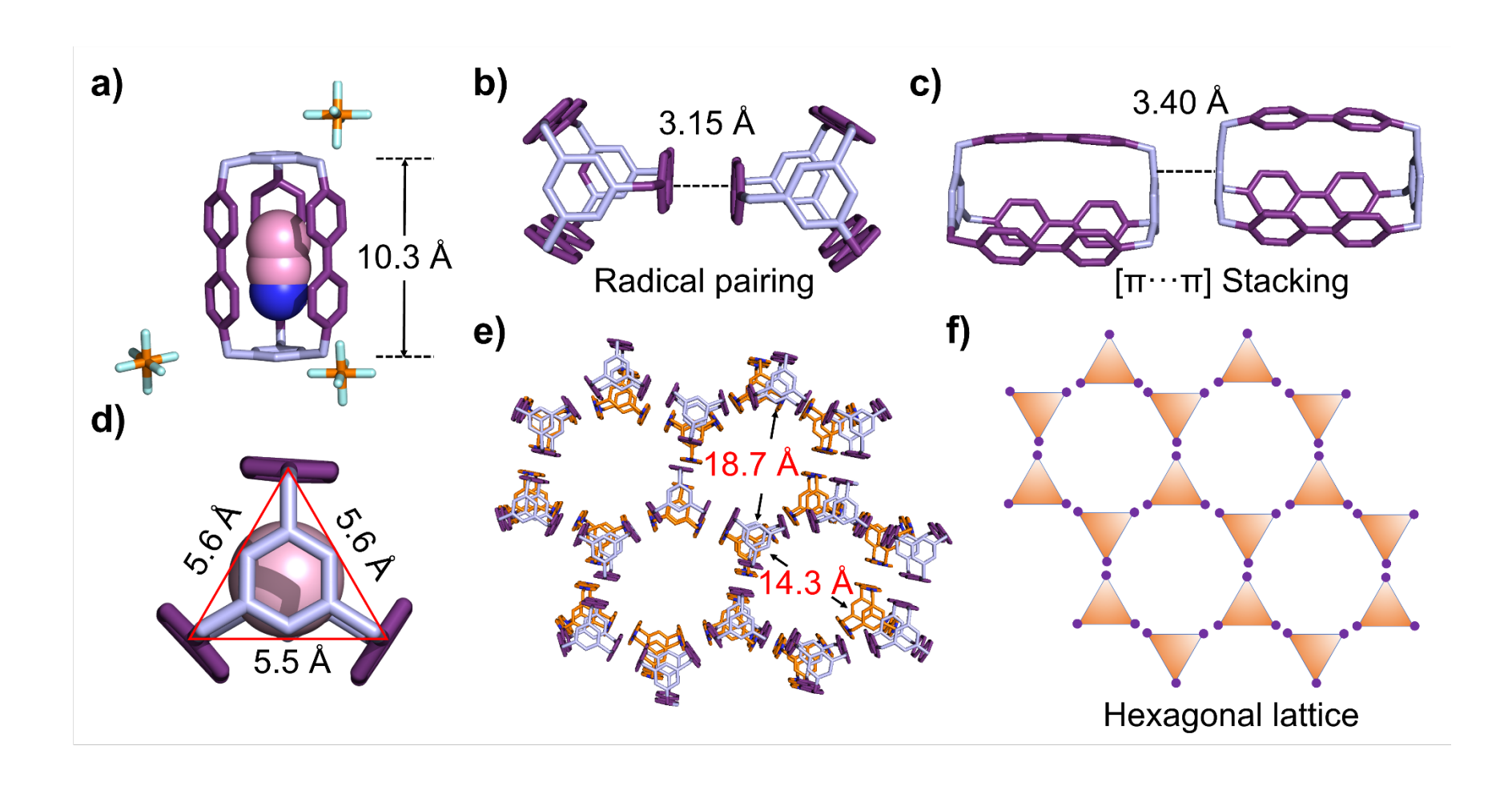


Figure 5

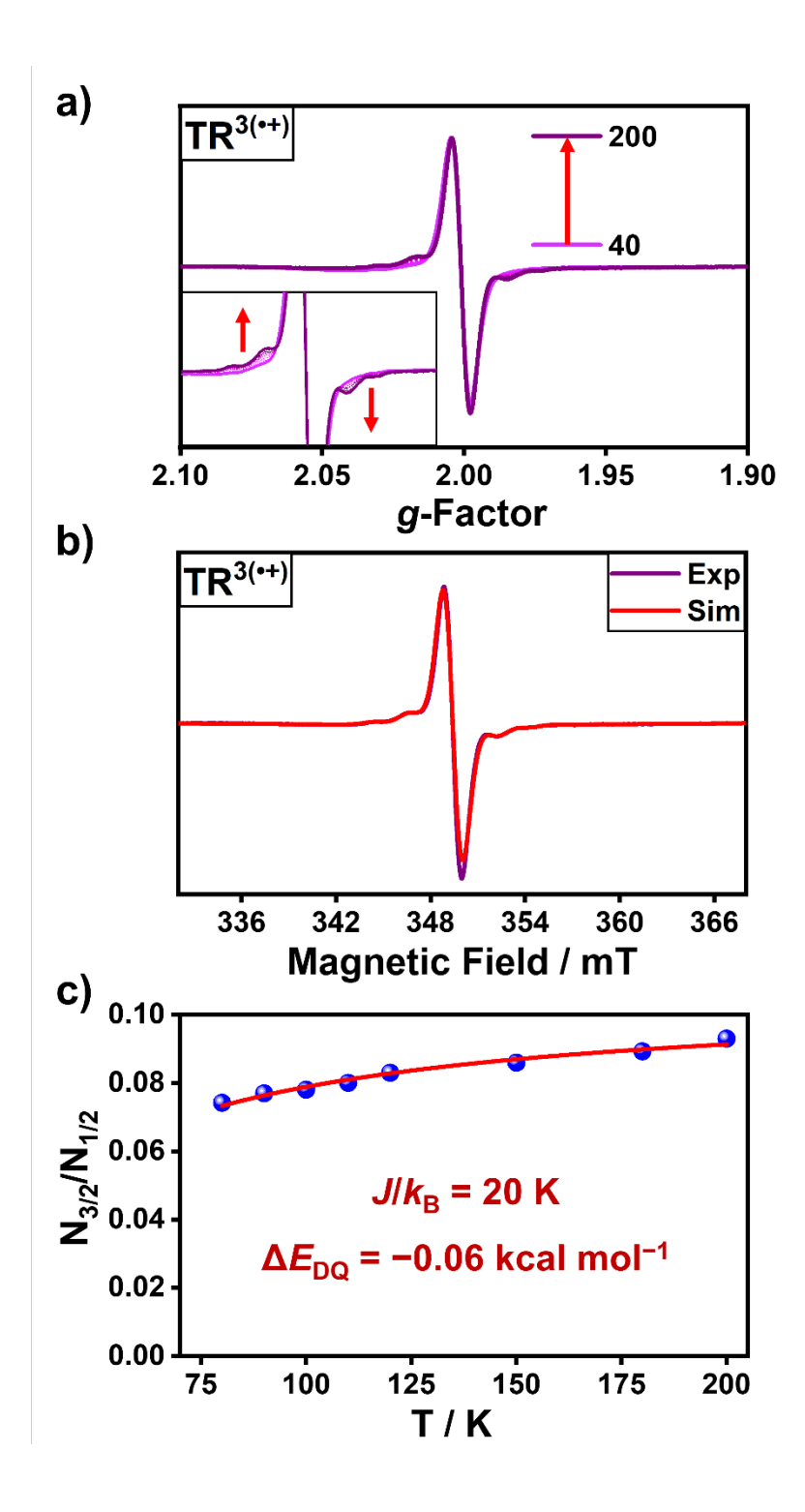


Figure 6

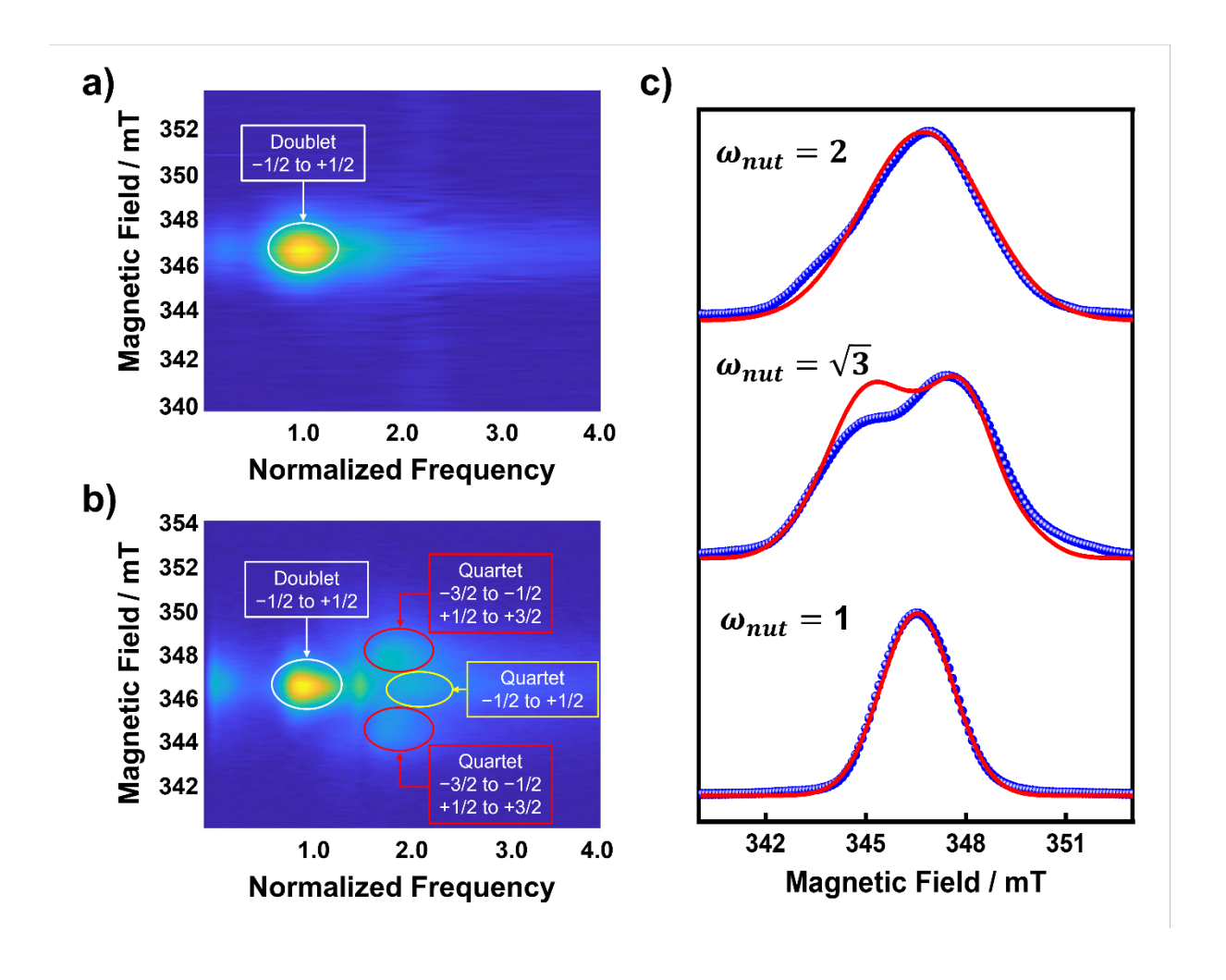


Figure 7

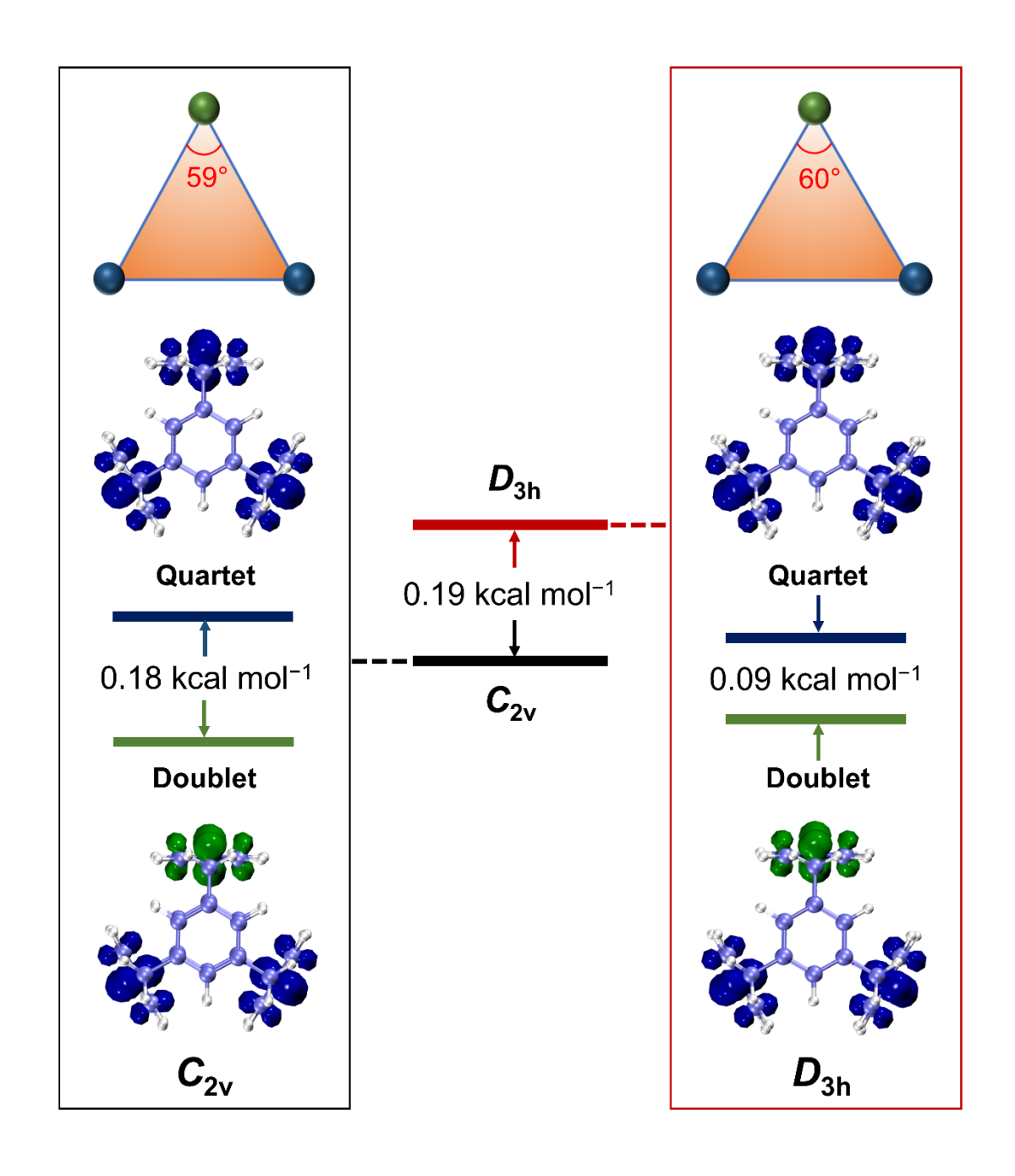
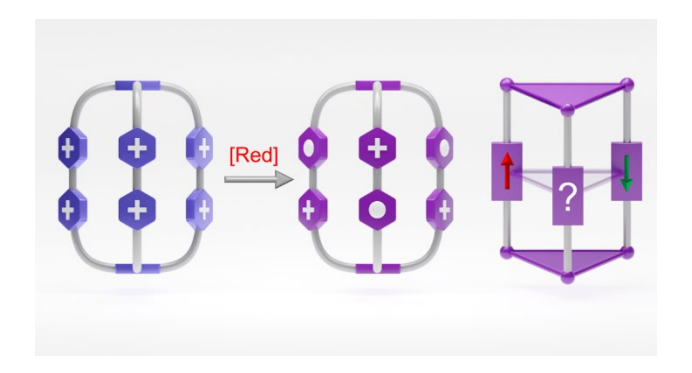


Figure 8



# **Table of Contents**